Monthly Notices of the ROYAL ASTRONOMICAL SOCIETY
MNRAS **451,** 312–322 (2015) doi:10.1093/mnras/stv971

The *Hubble Space Telescope* UV Legacy Survey of Galactic Globular Clusters – IV. Helium content and relative age of multiple stellar populations within NGC 6352⋆

D. Nardiello,[1,2,3†] G. Piotto,[1,2] A. P. Milone,[3] A. F. Marino,[3] L. R. Bedin,[2] J. Anderson,[4] A. Aparicio,[5,6] A. Bellini,[4] S. Cassisi,[7] F. D'Antona,[8] S. Hidalgo,[5,6] S. Ortolani,[1,2] A. Pietrinferni,[7] A. Renzini,[2] M. Salaris,[9] R. P. van der Marel[4] and E. Vesperini[10]

[1]*Dipartimento di Fisica e Astronomia 'Galileo Galilei', Università di Padova, Vicolo dell'Osservatorio 3, Padova I-35122, Italy*
[2]*Istituto Nazionale di Astrofisica – Osservatorio Astronomico di Padova, Vicolo dell'Osservatorio 5, Padova I-35122, Italy*
[3]*Research School of Astronomy and Astrophysics, The Australian National University, Cotter Road, Weston, ACT 2611, Australia*
[4]*Space Telescope Science Institute, 3800 San Martin Drive, Baltimore, MD 21218, USA*
[5]*Instituto de Astrofisica de Canarias, E-38200 La Laguna, Tenerife, Canary Islands, Spain*
[6]*Department of Astrophysics, University of La Laguna, E-38200 La Laguna, Tenerife, Canary Islands, Spain*
[7]*Istituto Nazionale di Astrofisica – Osservatorio Astronomico di Teramo, Via Mentore Maggini s.n.c., I-64100 Teramo, Italy*
[8]*Istituto Nazionale di Astrofisica - Osservatorio Astronomico di Roma, Via Frascati 33, I-00040 Monteporzio Catone, Roma, Italy*
[9]*Astrophysics Research Institute, Liverpool John Moores University, Liverpool Science Park, IC2 Building, 146 Brownlow Hill, Liverpool L3 5RF, UK*
[10]*Department of Astronomy, Indiana University, Bloomington, IN 47405, USA*

Accepted 2015 April 29. Received 2015 April 29; in original form 2015 April 15

ABSTRACT

In this paper, we combine Wide Field Camera3/UVIS *F*275*W*, *F*336*W*, and *F*438*W* data from the 'UV Legacy Survey of Galactic Globular Clusters: Shedding Light on Their Populations and Formation' (GO 13297) *Hubble Space Telescope* Treasury programme with *F*606*W*, *F*625*W*, *F*658*N*, and *F*814*W* Advanced Camera for Surveys archive data for a multiwavelength study of the globular cluster NGC 6352. In the colour–magnitude and two-colour diagrams obtained with appropriate combination of the photometry in the different bands, we separate two distinct stellar populations and trace them from the main sequence to the subgiant, red giant, horizontal and asymptotic giant branches. We infer that the two populations differ in He by $\Delta Y = 0.029 \pm 0.006$. With a new method, we also estimate the age difference between the two sequences. Assuming no difference in [Fe/H] and [α/Fe], and the uncertainties on ΔY, we found a difference in age between the two populations of 10 ± 120 Myr. If we assume [Fe/H] and [α/Fe] differences of 0.02 dex (well within the uncertainties of spectroscopic measurements), the total uncertainty in the relative age rises to ∼300 Myr.

Key words: techniques: photometric – stars: Population II – globular clusters: individual: NGC 6352.

1 INTRODUCTION

The *Hubble Space Telescope* (*HST*) 'UV Legacy Survey of Galactic Globular Clusters: Shedding Light on Their Populations and Formation' (GO 13297, PI Piotto) is a Treasury programme to study globular cluster (GC) stellar populations using multiwavelength high-precision *HST* photometry and astrometry. The programme is fully described in Piotto et al. (2015, hereafter Paper I). The main purpose of this survey is to identify multiple stellar populations and study their properties, including their relative ages, chemical compositions, spatial distributions, and kinematics. Within GO 13297, we collected *F*275*W*, *F*336*W*, and *F*438*W* WFC3/UVIS images, approximately overlapping the *F*606*W* and *F*814*W* data from GO 10755 (PI Sarajedini; see Sarajedini et al. 2007).

In this paper, we analyse photometry of stars in the Galactic GC NGC 6352. Our main purpose is to infer the helium content and determine the relative ages of its stellar populations. NGC 6352 is a Bulge (Galactic coordinates: $l = 341$, $b = -7.2$), metal-rich

⋆ Based on observations with the NASA/ESA *Hubble Space Telescope*, obtained at the Space Telescope Science Institute, which is operated by AURA, Inc., under NASA contract NAS 5-26555 under GO 13297.
†E-mail: domenico.nardiello@studenti.unipd.it

GC, located at 5.6 Kpc from the Sun [$(m - M)_V = 14.43$, $E(B - V) = 0.22$, Harris 1996, 2010 revision], and having luminosity $M_V = -6.47$ (Harris 1996, 2010 revision) and mass of 3.7×10^4 $M_\odot$ (Marks & Kroupa 2010). From high-resolution spectroscopy of nine horizontal branch (HB) stars, Feltzing, Primas & Johnson (2009) confirmed the results of previous works, that this cluster has a high metallicity ([Fe/H] ~ -0.55) and is α-enhanced ([α/Fe] ~ 0.2).

The paper is organized as follows. Section 2 presents the data and data analysis. Section 3 and 4 show the characteristics of the two stellar populations hosted by NGC 6352, and their properties as seen with different combinations of colours and magnitudes. In Section 5, the difference in the helium content of the two stellar populations is calculated. In Section 6, we describe the new method we developed to estimate the difference in age between the two stellar populations. In Section 7, there are the conclusions.

2 OBSERVATIONS AND DATA ANALYSIS

In order to identify the multiple stellar populations in NGC 6352, we used WFC3/UVIS images of GO 13297 and ACS/WFC data of GO 10775. The WFC3 data set consists in 2 ×706 s +2 × 800 s *F275W*, 4 × 311 s *F336W*, and a 58 s + 72 s *F438W* images. ACS data include 4 × 140 s + 7 s *F606W* and 4 × 150 s + 7 s *F814W* images, overlapped to WFC3 images. We also reduced ACS images collected in *F625W* and *F658N* bands within GO 12746 (PI Kong). Exposure times are 2×150 s in *F625W* and a 650 s + 643 s in *F658N*. A detailed description of the reduction of GO 13297 data is provided in Paper I (see their section 5). We have used the photometric and astrometric catalogues published by Anderson et al. (2008) for GO 10775 data, while photometry and astrometry of archive ACS/WFC images from GO 12746 have been carried out as in Anderson et al. (2008).

3 THE CMDs OF NGC 6352

In Paper I (see their fig. 2), we have shown that the colour–magnitude diagram (CMD) of NGC 6352 is not consistent with a single stellar population. The m_{F814W} versus $m_{F606W} - m_{F814W}$ CMD of the cluster members of NGC 6352 is shown in Fig. 1; in black there are the stars that, on the basis of their proper motions, have high probability to be cluster members, in light blue the rejected stars. To derive stellar proper motions, we determined the displacement between the stellar positions in GO 10775 data set (2006.4) and in GO 13297 data set (2013.7 and 2014.5) by following the method described in detail by Piotto et al. (2012, see their section 4). The maximum time baseline for the proper motion measurements is 8.1 yr.

Fig. 2(a) shows the m_{F606W} versus $C_{F275W,\,F336W,\,F438W} = (m_{F275W} - m_{F336W}) - (m_{F336W} - m_{F438W})$ diagram for proper-motion-selected cluster members. Asymptotic giant branch (AGB), stars selected from the m_{F336W} versus $m_{F336W} - m_{F814W}$ CMD, are represented with starred symbols. Two distinct sequences are clearly visible and can be continuously followed from the main sequence (MS), the subgiant branch (SGB), the red giant branch (RGB), to the HB, and the AGB. Panels (b)–(e) of Fig. 2 show a collection of CMDs for NGC 6352 and reveal the pattern of its multiple sequences.

3.1 Multiple stellar populations in NGC 6352

In Fig. 3, we use the m_{F336W}-m_{F438W} versus m_{F275W}-m_{F336W} two-colour diagram to separate the two populations, named population-a (POPa) and population-b (POPb) hereafter. Panel (a) of Fig. 3 shows

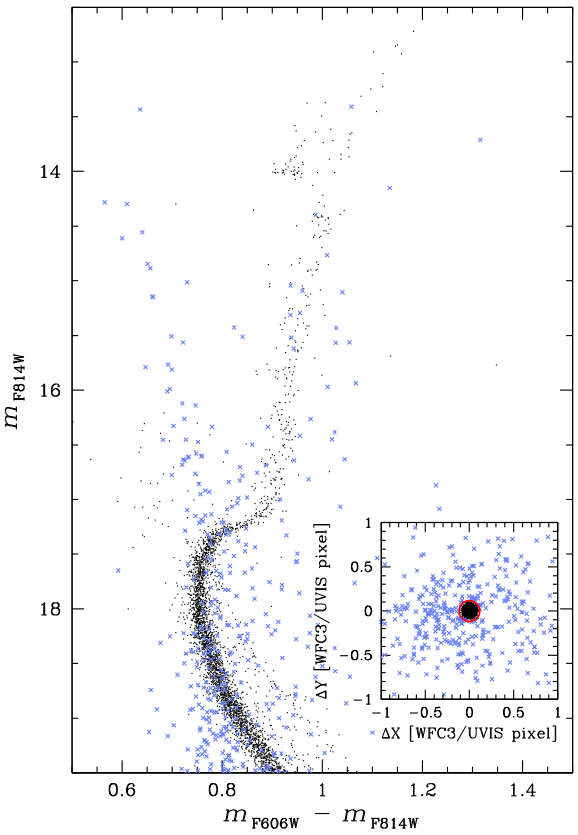

Figure 1. The m_{F814W} versus $m_{F606W} - m_{F814W}$ diagram of NGC 6352. In black and in light blue are plotted cluster members and field stars, respectively. Cluster members have been selected on the basis of their proper motions. The vector-points diagram of proper motions is plotted in the inset. Black points within red circle and light blue points outside red circle indicate members and field stars, respectively.

the m_{F814W} versus $m_{F606W} - m_{F814W}$ CMD, corrected for differential reddening and only for cluster-member stars, selected using proper motions. The green dotted lines identify the four regions in the CMD which include MS, SGB, RGB and HB stars. Again, AGB stars are plotted using starred symbols. All stars that, on the basis of their position on the CMD, are possible binaries, blue stragglers or survived field stars have been excluded from the following analysis and plotted as grey crosses.

Our recent papers demonstrated how two-colour and CMDs made with appropriate combination of far-ultraviolet, ultraviolet and blue magnitudes represent a very efficient tool to identify multiple stellar populations in a GC (Milone et al. 2012c,b, 2013; Paper I). Panels (b1), (b2), (b3), and (b4) of Fig. 3 show the $m_{F336W} - m_{F438W}$ versus $m_{F275W} - m_{F336W}$ two-colour diagrams for the four evolutionary sequences highlighted in the left-hand panel CMD. Two sequences are clearly visible in each diagram. We drew by hand a straight continuous line to separate the two groups of POPa and POPb stars in the SGB, RGB + AGB, and HB, and coloured them green and magenta, respectively. The two sequences of AGBa and AGBb stars are separated by the black dashed line in panel (b2). In order to separate the two MSs, we used the m_{F814W} versus $C_{F275W,\,F336W,\,F438W}$ diagram plotted in panel (c1) of Fig. 3. Indeed, in this pseudo-CMD the double MS of NGC 6352 is better distinguishable than in the $m_{F336W} - m_{F438W}$ versus $m_{F275W} - m_{F336W}$ plane.

The green and the magenta fiducial lines, superimposed on the MS, are the fiducials of the MSa and the MSb, respectively,

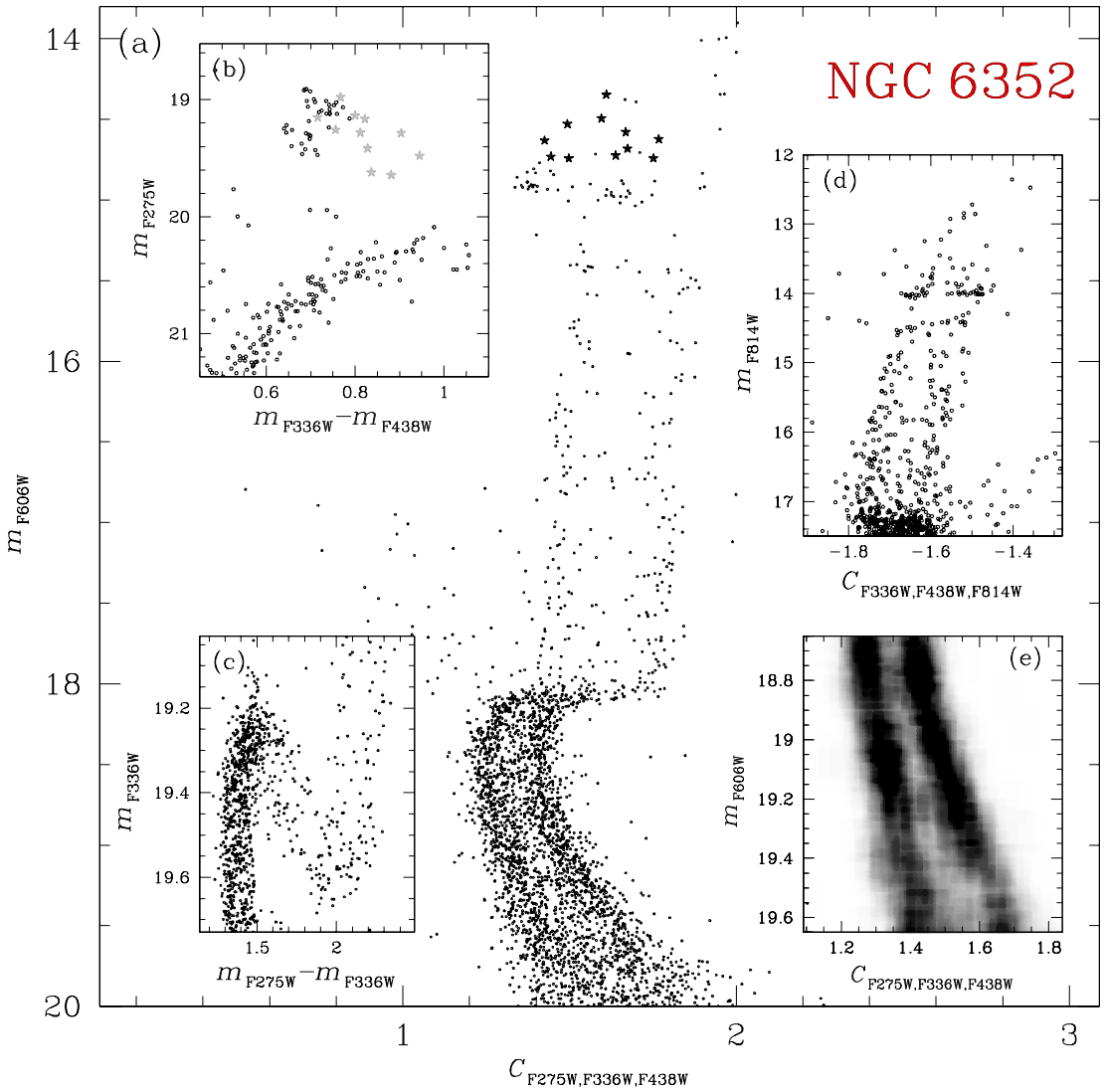

Figure 2. Overview of the main features in the CMDs of NGC 6352. Panel (a) shows the m_{F606W} versus $C_{F275W,\,F336W,\,F438W}$ pseudo-CMD, in which the split of all the sequences is clear (starred points represent the AGB stars); panel (b) shows the region around the HB in the m_{F275W} versus $m_{F336W} - m_{F438W}$ CMD; panel (c) highlights the SGB split in the m_{F336W} versus $m_{F275W} - m_{F336W}$ diagram; panel (d) shows the RGB region in the m_{F814W} versus $C_{F336W,\,F438W,\,F814W}$ pseudo-CMD. The Hess diagram of the MS stars shown in panel (a) is plotted in panel (e) and highlights the two distinct sequences.

and have been obtained by using the following procedure. As a first guess, we have selected by eye a sample of MSa and MSb stars and derived for each of them a fiducial line by fitting a spline through the median values of $C_{F275W,\,F336W,\,F438W}$ obtained in successive short intervals of magnitude. We iterated this step with a sigma-clipping procedure. Then, as in Milone et al. (2015, hereafter Paper II), we verticalized the MS in such a way that the green and magenta fiducials translate into vertical lines with abscissa $\Delta^{N}_{C_{F275W,F336W,F438W}} = 0$ and -1, respectively. The histogram of the distribution in $\Delta^{N}_{C_{F275W,F336W,F438W}}$ plotted in panel (c2) is clearly bimodal. We considered stars with $\Delta^{N}_{C_{F275W,F336W,F438W}} > -0.5$ as MSa members and the remaining MS stars as MSb objects. Panel (c3) shows the m_{F814W} versus $\Delta^{N}_{C_{F275W,F336W,F438W}}$ verticalized diagram for the MS stars. We coloured MSa and MSb stars in green and magenta, respectively. These colours will be consistently used hereafter.

3.2 The chemical composition of the HB stars

Typically, multiple sequences along the CMD correspond to distinct stellar populations with different content of helium and light elements (see e.g. Marino et al. 2008; Yong & Grundahl 2008; Paper II). Feltzing et al. (2009) measured chemical abundances for nine HB stars of NGC 6352 from high signal-to-noise spectra collected with the Ultraviolet and Visual Echelle Spectrograph (UVES) mounted at the Very Large Telescope (VLT). They have confirmed that NGC 6352 is a metal-rich GC ([Fe/H] $= -0.55 \pm 0.03$), and is enhanced in α elements by [α/Fe]$\sim$0.2 dex. Feltzing and collaborators also detected significant star-to-star sodium variation in close analogy with what is observed in most Milky Way GCs (e.g. Kraft et al. 1993; Gratton, Sneden & Carretta 2004).

In order to investigate the chemical content of POPa and POPb, we have exploited the spectroscopic results by Feltzing et al. (2009). Our photometric catalogue includes seven stars studied by Feltzing

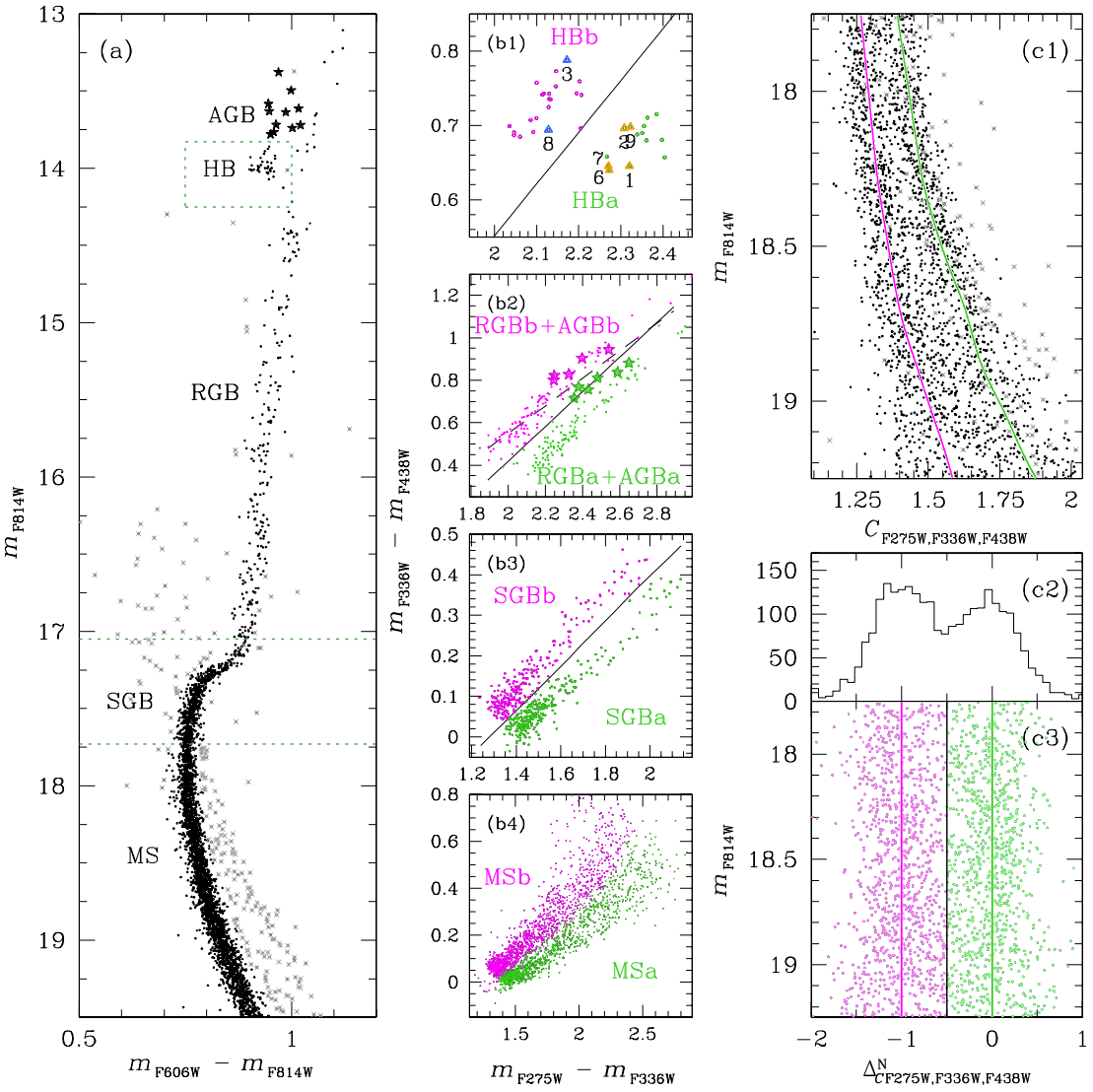

Figure 3. Procedure for the selection of POPa and POPb stars. Panel (a) shows the m_{F814W} versus $m_{F606W} - m_{F814W}$ CMD of NGC 6352: grey crosses are the stars that are possible binaries and blue stragglers and that are not used in this work. Panels (b) show the $m_{F336W} - m_{F438W}$ versus $m_{F275W} - m_{F336W}$ diagrams for MS, SGB, RGB, AGB and HB stars of POPa (green) and POPb (magenta). In panel (b1), we also plot the stars in common with the spectroscopic catalogue of Feltzing et al. (2009). Panels (c) show the procedure used for the selection of MSa and MSb stars (see the text for details).

et al. (2009). Five of them belong to the HBa and are Na-poor ([Na/H]≤−0.38). The other two are Na-rich ([Na/H]≥−0.27) and are HBb members. The two groups of Na-rich and Na-poor stars both have the same mean metallicity [Fe/H]=−0.55 ± 0.02. In panel (b1) of Fig. 3, we plotted these HB stars as triangles with the corresponding ID number adopted by Feltzing et al. (2009); orange triangles are for Na-poor stars, cyan triangles show the Na-rich ones.

4 MULTIWAVELENGTH VIEW OF MULTIPLE POPULATIONS

In the previous section, we used the m_{F814W} versus $C_{F275W,\,F336W,\,F438W}$ pseudo-CMD and the $m_{F336W}-m_{F438W}$ versus $m_{F275W}-m_{F336W}$ two-colour diagram, where multiple sequences are clearly distinguishable, in order to select the members of the two stellar populations along the MS, the SGB, the RGB, and the HB of NGC 6352. We can now combine all different bands in order to study the behaviour (e.g. colour differences) of the two populations in all possible CMDs we can construct with our data. An example is shown in Fig. 4. Note that POPa stars are redder than POPb ones in the m_{F275W} versus $m_{F275W}-m_{F336W}$ CMD, while they are bluer in the m_{F336W} versus $m_{F336W}-m_{F438W}$ CMD, as in the case of 47 Tuc (Milone et al. 2012b). The two upper panels of Fig. 5 show the m_{F814W} versus $m_X - m_{F814W}$ fiducial lines for the RGBs (top panels) and MSs (middle panels) of the two populations, where $X = F275W$, $F336W$, $F438W$, $F606W$, $F625W$, and $F658N$.

POPa is redder than POPb in most of the CMDs of Fig. 5, in close analogy with what is observed in most GCs (Bellini et al. 2010; Milone et al. 2012c,b, 2013). In visual and ultraviolet the $m_X - m_{F814W}$ colour separation between POPa and POPb increases with the colour baseline, and is maximum for $m_{F275W} - m_{F814W}$. The fiducial of the two populations are almost coincident in $m_{F336W}-m_{F814W}$, where POPa is slightly bluer than POPb.

The procedure used to determine each fiducial line is based on the naive estimator (Silverman 1986). First, we defined a series of

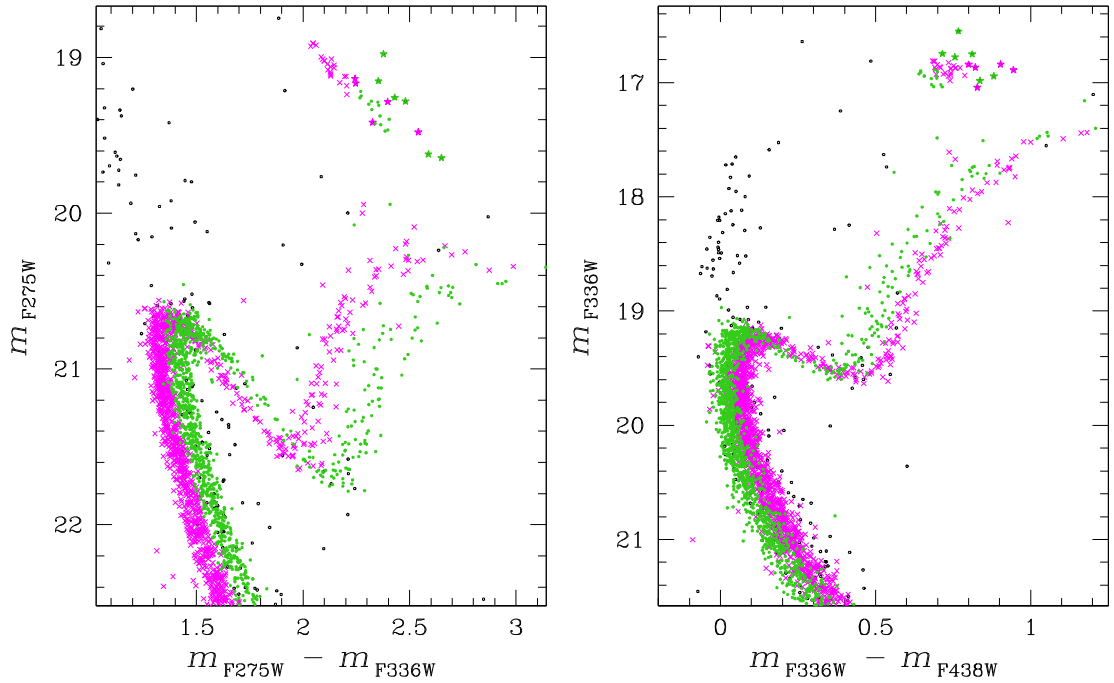

Figure 4. The m_{F275W} versus $m_{F275W}-m_{F336W}$ (left-hand panel) and m_{F336W} versus $m_{F336W}-m_{F438W}$ (right-hand panel) CMDs. In the first CMD, POPa stars (green dots) are redder than POPb stars (magenta crosses), while in the m_{F336W} versus $m_{F336W}-m_{F438W}$ CMD POPa stars have, on average, bluer colours than POPb stars.

N m_{F814W} magnitude intervals with a given width (w). Magnitude intervals are defined over a grid of N points separated by step of fixed magnitude (s). We calculated the median magnitude $m_{F814W,\,i}$ and colour $(m_X - m_{F814W})_i$ of stars within each magnitude interval $i = 1, \ldots, N$. These median points have been smoothed using the smoothing technique of boxcar averaging, in which each point of a vector is replaced with the average of the M adjacent points. Finally, the smoothed median points were interpolated with a cubic spline.

The choice of w is the result of a compromise. On one hand, we require small magnitude intervals to account for the detailed structure of the fiducial line. On the other hand, we need a large width to include in the magnitude interval a large number of stars for a statistically significant measurement of the median colour and magnitude. We used different values of w for stars with different luminosity. Specifically, we assumed $w = 0.5$ for RGB stars with $15.00 \leq m_{F814W} < 17.00$, $w = 0.25$ for SGB stars with $17.00 \leq m_{F814W} < 17.75$, and $w = 0.05$ for MS stars with $17.75 \leq m_{F814W} < 19.00$. In all the cases, we used $s = w/3$.

In order to estimate the error associated with the colours ($\sigma_{\rm fidcol}$) and magnitudes ($\sigma_{\rm fidmag}$) of each observed fiducial, we used the following procedure. For each stellar population selected in Fig. 3, we assigned a subsample of artificial stars (ASs) and randomly extracted a star from it by following the recipe in Milone et al. (2009). The AS subsample consists of all the ASs with similar magnitudes (within 0.3 m_{F814W} magnitudes) and radial distances (less than 100 pixels from the observed star). This method produces a catalogue of simulated stars with almost the same luminosity and radial distribution of the observed catalogue. We applied the procedure described above to estimate the fiducial line of the sample of AS stars, and calculated the difference between the fiducial of the ASs and the real stars. We repeated this step 100 times. The colour error associated with each point of the observed fiducial is calculated as the 68.27th percentile of this distribution.

5 THE HELIUM ABUNDANCE OF THE TWO STELLAR POPULATIONS

The helium abundance of a stellar population is a fundamental ingredient to understand its evolution, and to shed light on the chemical-enrichment and the star formation history in a GC. In addition, accurate helium determination is crucial to estimate several parameters of the host star cluster, like age, mass, and mass function.

A direct spectroscopic determination of the He content in GCs is only feasible in rare cases and for a tiny subset of stars (e.g. Behr 2003; Villanova, Piotto & Gratton 2009; Dupree, Strader & Smith 2011; Pasquini et al. 2011; Marino et al. 2014). On the other hand, the method based on multiwavelength photometry of multiple sequences that we developed can be applied to all clusters and provides a reliable estimate of the He abundance differences among the different populations and can reach internal errors smaller then spectroscopic methods (see Milone et al. 2012b; Paper II and references therein). In the few cases where helium has been inferred from both spectroscopy of HB stars and photometry, the results from the two techniques are in fairly agreement. In the case of NGC 2808, Marino et al. (2014) derived an helium abundance $Y = 0.34 \pm 0.01 \pm 0.05$ (internal plus systematic uncertainty) from spectroscopy of HB stars slightly bluer than the RR Lyrae instability strip. This result is consistent with the helium abundance inferred from the analysis of multiple MSs, where the middle MS (which would be associated with the stars analysed by Marino and collaborators), has $Y \sim 0.32$ (Piotto et al. 2007; Milone et al. 2012a). Similarly in the case of NGC 6397, both photometry (di Criscienzo, D'Antona & Ventura 2010; Milone et al. 2012c) and spectroscopy (Mucciarelli et al. 2014) conclude that second-population stars are slightly enhanced in Y by $\Delta Y \sim 0.01$ dex. In the case of M 4, Villanova et al. (2012) found that the second population is enhanced in helium by 0.04–0.05 dex with respect to the first one. This result is in apparent disagreement with results by Nardiello et al. (2015) who inferred

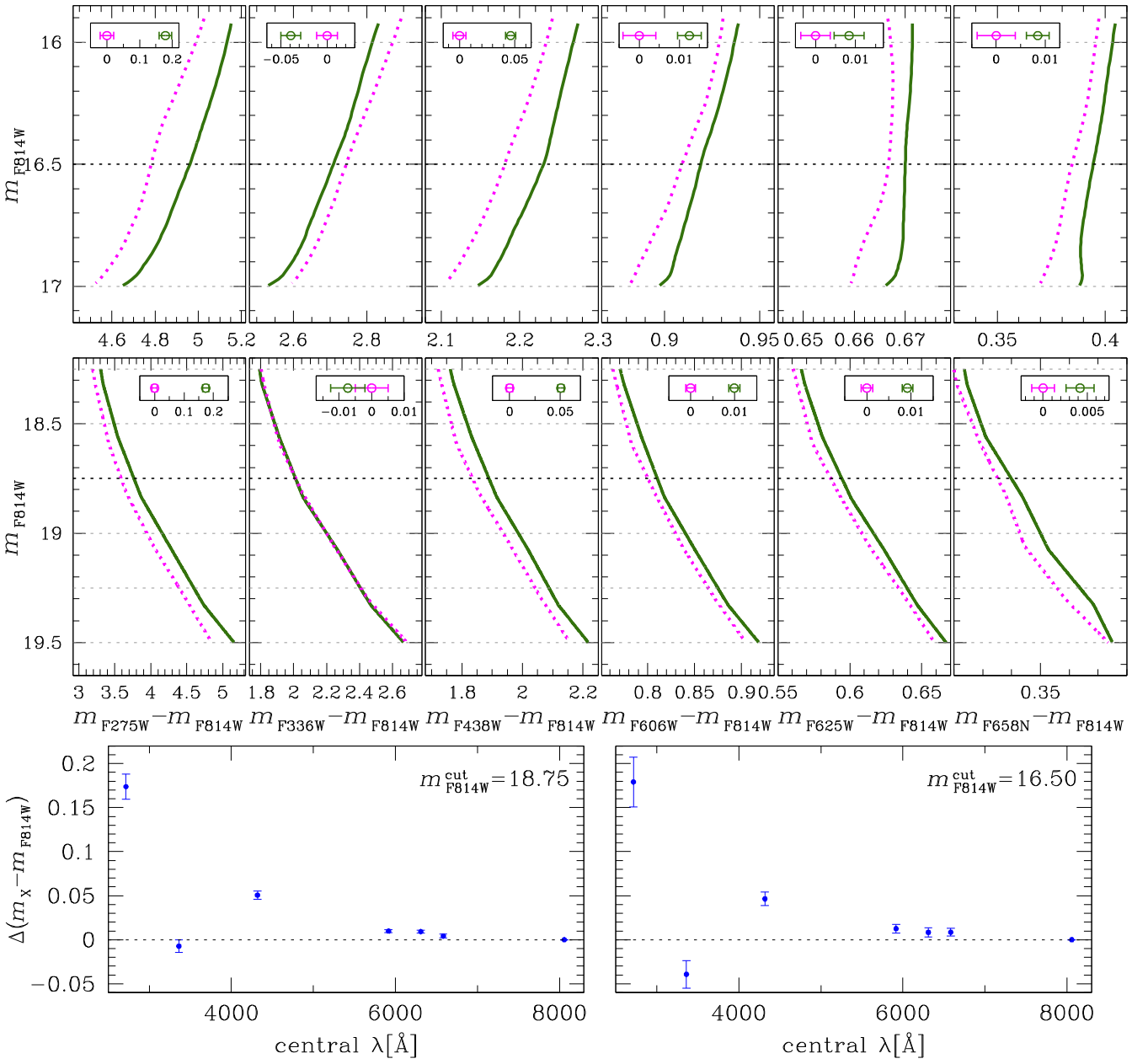

Figure 5. Top panels: RGB fiducial lines for POPa (green solid lines) and POPb (magenta dotted lines) in six m_{F814W} versus $m_X - m_{F814W}$ CMDs (where $X = F275W, F336W, F438W, F606W, F625W, F658N$); the panel insets show the colour distance between the two fiducials at $m^{\rm CUT}_{F814W} = 16.5$. Middle panels: same as top panels, but for the MS; the colour difference indicated in the inset is measured at $m^{\rm CUT}_{F814W} = 18.75$. Bottom panels: $m_X - m_{F814W}$ colour distance between MSa and MSb at $m^{\rm CUT}_{F814W} = 18.75$ (*left*) and between RGBa and RGBb at $m^{\rm CUT}_{F814W} = 16.50$ (*right*) as a function of the central wavelength of the X filter.

an helium difference of 0.020 ± 0.008 dex between the two MSs of this clusters. However, it should be noted that the discrepancy could be due to Non Local Thermodynamic Equilibrium that affect the helium line at 5875.6 Å (see e.g. Marino et al. 2014, Section 4 for the case of NGC 2808).

Helium has been also inferred in RGB stars from near-infrared chromospheric transition of He I at 10 830 Å in NGC 2808 and ω Centauri. The spectra suggest helium abundances of Y <0.22 and Y =0.39–0.44 ($\Delta Y \geq 0.17$) for the two analysed stars in ω Centauri (Dupree & Avrett 2013), while Na-rich and Na-poor stars of NGC 2808 analysed by Pasquini et al. (2011) differ in helium by ΔY >0.17, with the sodium-rich star being also helium rich. Such helium variation are larger than those obtained from the analysis of multiple sequences in the CMD that are ∼0.07 for NGC 2808 (D'Antona et al. 2005; Piotto et al. 2007; Milone et al. 2012a) and ∼0.13 for ω Centauri (King et al. 2012).

Fig. 5 illustrates the procedure to infer the helium content of the stellar populations in NGC 6352. Upper panels show a collection of m_{F814W} versus $m_X - m_{F814W}$ fiducial lines, where $X = F275W$, $F336W$, $F438W$, $F606W$, $F625W$ and $F658N$. We have used green and magenta continuous lines to plot the fiducials along the RGB (top panels) and the MS (middle panels) of the two populations. We have calculated the colour difference between the green and the magenta fiducials at the reference magnitudes indicated by the black

dashed lines at $m^{\rm CUT}_{F814W} = 18.75$ for the MS, and $m^{\rm CUT}_{F814W} = 16.50$ for the RGB.

Results are shown in the lower panels of Fig. 5. We found that $\Delta(m_X - m_{F814W})$ has negative values only for $X = F336W$. When the other filters are used, the $m_X - m_{F814W}$ colour separation between the two RGBs and MSs is maximum for $X = m_{F275W}$ and decreases towards redder wavelengths of the X filter.

In order to estimate the effective temperatures ($T_{\rm eff}$) and gravities ($\log g$) of MS and RGB stars with $m_{F814W} = m^{\rm CUT}_{F814W}$, we used the isochrones by Dotter et al. (2008) that best match the CMD.

Note that we are mainly interested in relative ages rather than in absolute ones. Indeed, as demonstrated in next section, accurate relative ages are feasible using our data set. Here, we just need reference models to calculate the colour differences of the two populations. As discussed in Section 6, the best match with observations could be obtained using isochrones with [Fe/H] $= -0.67$, in fair agreement with the value inferred from high-resolution spectroscopy by Carretta & Gratton (1997), [α/Fe] $= 0.4$, and an age of 13.1 Gyr [adopting $(m - M)_V = 14.43$, an $E(B - V) = 0.22$; Harris 1996, 2010 edition]. We assumed $Y = 0.256$ for POPa, and different helium abundances with Y ranging from 0.256 to 0.330, in steps of 0.001, for POPb. Since there are no measurements of C, N, O abundance for NGC 6352 stars, we assumed for POPa and POPb the same C, N, O content as the two main stellar populations of 47 Tuc. Specifically, we used for POPa [C/Fe] $= -0.20$, [N/Fe] $= 0.20$, [O/Fe] $= 0.40$, and assumed that POPb stars are depleted in carbon and oxygen by 0.20 and 0.15 dex, respectively, and nitrogen enhanced by 0.7 dex with respect to POPa stars.

We used the ATLAS12 code (Kurucz 1993; Sbordone et al. 2004) to calculate atmospheric models for the MS and RGB stars with $m_{F814W} = m^{\rm CUT}_{F814W}$, while synthetic spectra have been generated with SYNTHE (Kurucz & Avrett 1981) with a resolution of $R = 600$ from 2000 to 10 000Å.

Synthetic spectra of POPa and POPb stars have been integrated over the transmission curves of the WFC3/UVIS and the ACS/WFC filters used in this paper in order to determine synthetic colours. The colours from synthetic spectra with different Y have been compared with observations in order to estimate the helium abundance of POPb.

The best fit between observed and theoretical colours at $m^{\rm CUT}_{F814W}$ =18.75 can be obtained assuming POPb enhanced in helium by $\Delta Y = 0.033$ dex. We have repeated this procedure for $m^{\rm CUT}_{F814W}$ =18.25, 18.50, 19.00, 19.25, and 19.50 for the MS, and $m^{\rm CUT}_{F814W}$ =16.00, 16.50 and 17.00 for the RGB. The results are listed in Table 1. The values of $T_{\rm eff}$, $\log(g)$, and ΔY that provide the best fit to the observed colour differences are listed in Table 2 for each value of $m^{\rm CUT}_{F814W}$. On average, we have $\Delta Y = 0.029 \pm 0.006$, where the error represent the 68.27th percentile of the distribution of the sorted residuals from the mean value. To estimate ΔY, we only used visual bands ($F606W$, $F625W$, $F658N$, and $F814W$), because they are not affected by light-elements variations. For this reason, the final result is not conditioned by the assumptions on the C, N, and O abundances. In the case where C, N, and O abundances were known, the final value of ΔY, obtained using all the photometric bands, would not change. As a test, we repeated the procedure described above by assuming different values of C, N, and O; we found the same result.

6 RELATIVE AGES OF THE TWO STELLAR POPULATIONS

The relative ages of the multiple stellar populations hosted by GCs is an important issue to understand how GCs formed. We can speculate that the phenomenon of multiple stellar populations in GCs is due to the presence of different generations of stars, formed in different epochs: a first stellar generation (FG) characterized by primordial

Table 1. Colour difference $\Delta m_{X,\,F814W}$ at different $m^{\rm CUT}_{F814W}$.

$m^{\rm CUT}_{F814W}$	$\Delta m_{F275W,\,F814W}$	$\Delta m_{F336W,\,F814W}$	$\Delta m_{F438W,\,F814W}$	$\Delta m_{F606W,\,F814W}$	$\Delta m_{F625W,\,F814W}$	$\Delta m_{F658N,\,F814W}$
19.50	0.300 ± 0.028	-0.016 ± 0.017	0.049 ± 0.011	0.012 ± 0.003	0.005 ± 0.004	0.001 ± 0.004
19.25	0.234 ± 0.026	-0.009 ± 0.012	0.045 ± 0.007	0.011 ± 0.002	0.006 ± 0.003	0.005 ± 0.003
19.00	0.204 ± 0.019	-0.003 ± 0.009	0.048 ± 0.006	0.012 ± 0.002	0.009 ± 0.002	0.005 ± 0.003
18.75	0.174 ± 0.014	-0.007 ± 0.007	0.051 ± 0.005	0.010 ± 0.002	0.009 ± 0.002	0.004 ± 0.002
18.50	0.128 ± 0.011	-0.011 ± 0.006	0.045 ± 0.004	0.007 ± 0.002	0.005 ± 0.002	0.001 ± 0.002
18.25	0.111 ± 0.008	-0.008 ± 0.004	0.038 ± 0.003	0.008 ± 0.001	0.005 ± 0.001	0.001 ± 0.002
17.00	0.168 ± 0.038	-0.056 ± 0.030	0.052 ± 0.018	0.016 ± 0.008	0.016 ± 0.008	0.022 ± 0.009
16.50	0.179 ± 0.028	-0.039 ± 0.016	0.046 ± 0.008	0.013 ± 0.005	0.008 ± 0.005	0.009 ± 0.005
16.00	0.158 ± 0.030	-0.033 ± 0.020	0.044 ± 0.008	0.011 ± 0.005	0.010 ± 0.007	0.010 ± 0.006

Table 2. Parameters used to simulate synthetic spectra of POPa and POPb stars and estimation of helium difference between the two populations for different $m^{\rm CUT}_{F814W}$.

$m^{\rm CUT}_{F814W}$	$T_{\rm EFF,\,POPa}$	$T_{\rm EFF,\,POPb}$	$\log g_{\rm POPa}$	$\log g_{\rm POPb}$	ΔY
19.50	3673	3677	2.51	2.53	0.018
19.25	3678	3684	2.64	2.69	0.023
19.00	3687	3692	2.86	2.91	0.030
18.75	3693	3698	3.06	3.10	0.033
18.50	3698	3702	3.23	3.26	0.024
18.25	3700	3705	3.37	3.40	0.031
17.00	3766	3767	4.25	4.26	0.042
16.50	3764	3766	4.29	4.30	0.026
16.00	3754	3756	4.40	4.41	0.030
					0.029 ± 0.006

helium and chemical composition similar to that of field stars with the same metallicity, and a helium-enhanced second generation (SG), characterized by stars depleted in C and O and enhanced in N and Na, born from material processed at high temperature by FG stars. If we exclude the 'anomalous' GCs, such as ω Cen (Norris & Da Costa 1995), M 22 (Marino et al. 2011), and M 2 (Yong et al. 2014, Paper II), stars of different populations in 'normal' GCs show negligible differences in metallicity (Carretta et al. 2009). Because of this, we can exclude supernova ejecta as possible polluters of the material from which SG stars formed.

Current scenarios for the formation of multiple stellar populations in GCs predict different time-scales. The AGB scenario (D'Antona et al. 2002) predicts that envelopes of intermediate mass AGB stars are the cause of pollution. In models aimed at reproducing the observed chemical patterns in 'normal' GCs with AGB ejecta, the SG star formation epoch extends between about 40 and 90–100 Myr (D'Ercole et al. 2010, 2012). Another suggested mechanism is the formation of stars from material ejected by fast-rotating massive stars (FRMS) during the phase of core H-burning (Decressin et al. 2007) or massive binaries (Bastian et al. 2013; Salaris & Cassisi 2014). In these cases, the time-scale for the formation of the SG must be of the order of a few million years or even less (Bastian et al. 2013; D'Antona et al. 2014; Salaris & Cassisi 2014).

In this work, we present a method to set upper limits on the difference in age between the two populations of NGC 6352. For the first time, we estimate the relative age of two stellar populations in a normal GC, i.e. with no internal variation in [Fe/H]. Note that we are interested in measuring relative ages. The corresponding absolute ages should be only regarded as indicative (depending on the adopted distance modulus and reddening, as well as the reference model).

We consider a set of isochrones characterized by [Fe/H] $= -0.67$ and [α/Fe] $= 0.4$, that are the values that best fit all the stars in the m_{F814W} versus $m_{F606W} - m_{F814W}$, as explained in Section 5.

We also used the m_{F814W} versus $m_{F606W} - m_{F814W}$ CMD for computing the relative ages between the two populations, because in these filters the effect of light elements variation is not significant (Sbordone et al. 2011; Milone et al. 2012b). The MS turn-off is the classical age indicator of a simple stellar population. For this reason, we considered a region of the CMD around the MS turn-off of the two populations (panel a of Fig. 6). We obtained fiducials and the associated errors in colour and magnitudes (coloured regions between dashed lines) for POPa (green) and POPb (magenta) using the same procedure described in Section 4.

In order to compute the relative age between the two populations, we treated POPa and POPb as simple stellar populations and measured their ages independently. The age of each population is estimated by comparing the observed m_{F814W} versus $m_{F606W} - m_{F814W}$ CMD with a grid of synthetic CMDs with the same [Fe/H], [α/Fe] and Y, and ages that run from 12 000 to 15 000 Myr, in step of 50 Myr.

For each isochrone, a synthetic CMD was built in this way: we obtained a first guess synthetic CMD by interpolating the isochrone on the observed magnitudes, in such a way that to each m_{F814W} magnitude in the catalogue of real stars is associated a colour $m_{F606W} - m_{F814W}$ on the isochrone. In second step, we broadened this synthetic CMD by adding to the colour and magnitude of each synthetic star a random Gaussian error, with a dispersion equal to the error of the associated real star. The final result is a synthetic CMD, characterized by the same number of stars and a similar luminosity function to that of the observed CMD.

Panels (b) and (c) of Fig. 6 show an example of isochrones and corresponding synthetic CMDs. For each synthetic CMD, we computed the fiducial line using the same procedure as for the observed data. For each step in age, we built $N = 100$ synthetic simple stellar population CMDs, obtained the fiducial lines and computed the average of all the 100 fiducial lines in order to obtain the final synthetic fiducial line.

We compared the observed fiducial line of each population with the synthetic ones. This method is more robust than the direct comparison between the observed CMD and the isochrones, because we compared observed and theoretical fiducial lines which were computed in the same way and are affected by the same systematic errors introduced by the method (as, e.g. the error due to the smoothing). For each step in age, we calculated the χ^2 of the best fit between the synthetic and the observed fiducial, in a magnitude interval $17.00 < m_{F814W} < 18.2$. We fitted the χ^2 as a function of the age with a second-order polynomial, in order to find the age that minimizes the χ^2. This fit was performed in two steps: first, we fitted all the points with a parabola to obtain a first-guess value of the age, $t^{\rm I}$, that minimizes the χ^2 (panels d_1 and e_1 of Fig. 6). Then we considered only the points inside an interval between $t^{\rm I} - 500$ Myr and $t^{\rm I} + 500$ Myr and fitted a new second-order polynomial (panels d_2 and e_2) to find the best value that minimizes the χ^2.

We independently run this procedure for POPa and POPb. For POPa, we used a set of isochrones calculated for [Fe/H]$=-0.67$, [α/Fe] $= +0.4$ and $Y = 0.256$, while for POPb we used isochrones with the same metallicity and α-enhancement, but enhanced in helium by $\Delta Y = 0.029$ (i.e. with $Y = 0.285$) as obtained in Section 5. The best fit gives an age of (13 580 $\pm$ 80) Myr for POPa and (13 570 $\pm$ 80) Myr for POPb. We want to emphasize the fact that absolute ages are not significant in this context, and that we are interested only to relative ages. For this reason, hereafter we provide only relative ages. The age error is given by $\sigma = \sqrt{\sigma^2_{\rm PHOT} + \sigma^2_{\rm FIT}}$, where $\sigma_{\rm PHOT}$ is the error due to photometric errors and $\sigma_{\rm FIT}$ is the error on the fit of the χ^2 values.

The error due to photometry has been computed by performing the same analysis as described above and shifting the observed fiducial line in colour by a quantity equal to $\pm\sigma_{\rm fidcol}$ and in magnitude by a quantity equal to $\pm\sigma_{\rm fidmag}$. To estimate $\sigma_{\rm FIT}$, we used the bootstrap re-sampling of the data to generate 1000 samples randomly drawn from the original data sets; for each sample, we calculated the age that minimize the χ^2 as above described. Finally, we computed the mean age and its standard deviation, and adopted the latter as the uncertainty in the χ^2 fit. In conclusion, the two populations have a difference in age $\Delta_{\rm AGE} = {\rm AGE}_{\rm POPa} - {\rm AGE}_{\rm POPb} = (10 \pm 110)$ Myr.

Fig. 6 shows the whole procedure: in panel (a), we plot the CMDs of POPa and POPb (light green and magenta) and their fiducial lines. In panel (b), the best-fitting isochrones are plotted for each population; these are the isochrones for which the corresponding synthetic fiducials, shown in panel (c) with the synthetic CMDs, give the minimum χ^2. Panels (d) and (e) show the procedure adopted for the fit of the χ^2 for POPa and POPb, respectively. In panels (d_1) and (e_1) are shown the first guess fits (blue dashed lines), while in panels (d_2) and (e_2) show the final fits (green and magenta curves for POPa and POPb, respectively). The vertical dashed lines represent the value of the age that minimizes the χ^2.

We performed the same analysis using CMDs with different colour bases: $m_{F625W} - m_{F814W}$ and $m_{F658N} - m_{F814W}$. These CMDs are characterized by larger photometric errors. We found $\Delta_{\rm AGE} = 80 \pm 140$ Myr in the case of the m_{F814W} versus $m_{F625W} - m_{F814W}$ CMD, and $\Delta_{\rm AGE} = 220 \pm 210$ Myr in the case of the m_{F814W} versus $m_{F658N} - m_{F814W}$ CMD. The results are consistent

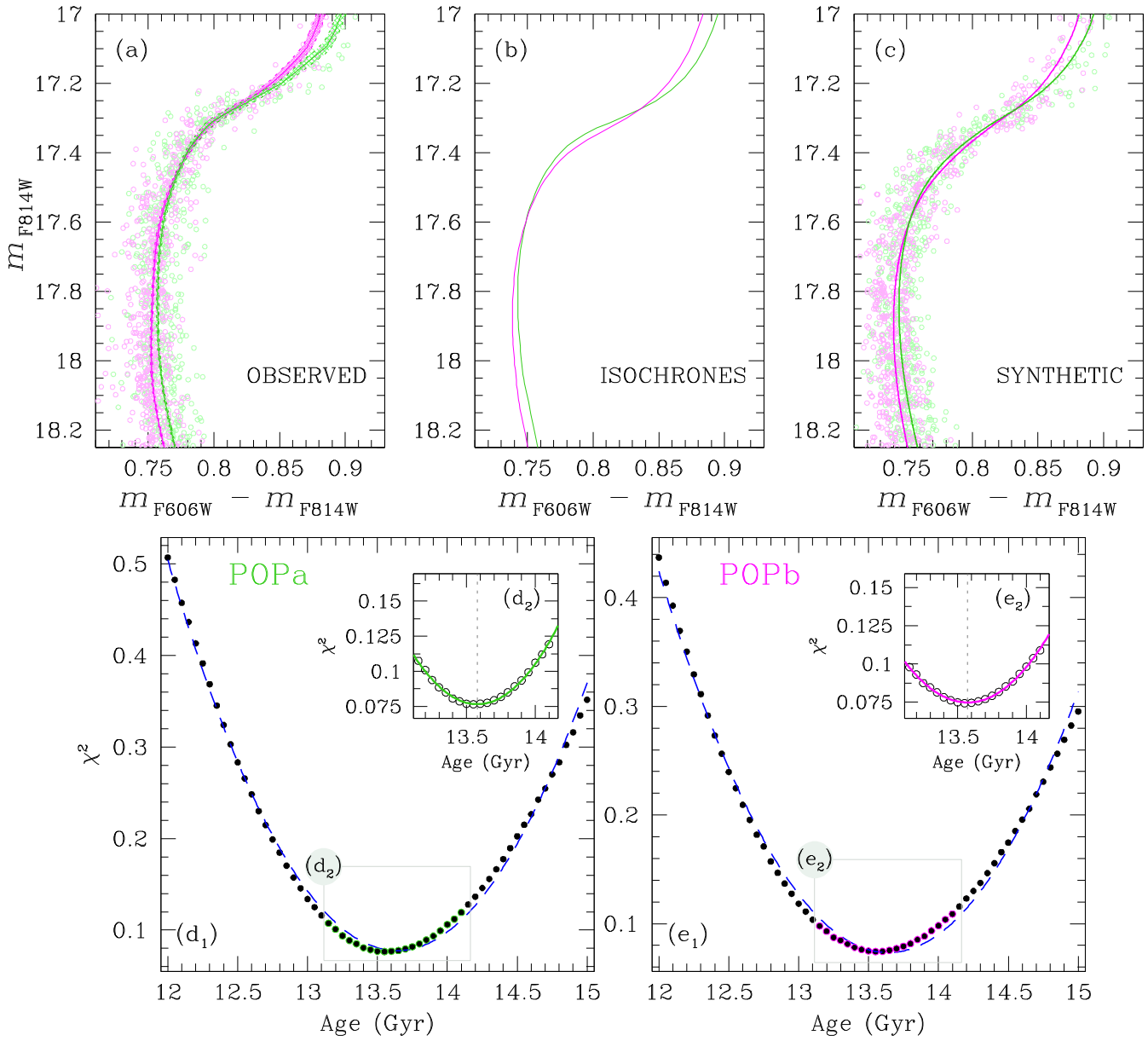

Figure 6. Procedure used to obtain the relative age of the two populations. In panel (a), the observed m_{F814W} versus $m_{F606W} - m_{F814W}$ CMD is shown. In green and magenta are the fiducial lines of the POPa and POPb, respectively. Panel (b) shows the best-fitting isochrones for the two populations, while in panel (c) we plot the synthetic CMD and the fiducial lines built using the isochrones calculated for the two population. Panels (d) and (e) illustrate the procedure adopted to derive the age of POPa and POPb, respectively. In panels (d_1) and (e_1), filled circles indicate the values of χ^2 for different ages while the dashed lines are the first-guess second-order polynomial fit. The insets (d_2) and (e_2) show the best-fitting second-order polynomial for POPa (green) and POPb (magenta, see the text for details).

with what found using the m_{F814W} versus $m_{F606W} - m_{F814W}$, but errors due to photometric uncertainties are larger. For this reason, we decided to carry out further analysis only using the m_{F814W} versus $m_{F606W} - m_{F814W}$ CMD.

We tested whether our results depend on the adopted magnitude interval for the fit. We iterated the procedure described above by changing the starting point of the magnitude interval between $m_{F814W} = 17.80$ and $m_{F814W} = 18.10$, and the ending point between $m_{F814W} = 17.00$ and $m_{F814W} = 17.30$, with steps of 0.05 mag. Within 50 Myr, we found no difference in the average age. Such age difference is consistent with zero within our measurement errors.

We tested our results using a different data set of isochrones, to prove that results are independent from adopted models. We considered BaSTI isochrones (Pietrinferni et al. 2004, 2009) and we performed the same analysis described above. We obtained a difference in age between the two populations of (-80 ± 110) Myr, in agreement with the results obtained previously.

There is some dispersion among the abundance measurements of NGC 6352 in the literature (see Feltzing et al. 2009 and discussion therein). Therefore, we re-iterated the same analysis using another set of isochrones with different [Fe/H] and [α/Fe]. Following the spectroscopic results by Feltzing et al. (2009), we considered a set of isochrones with [Fe/H] $= -0.55$ and [α/Fe] $= +0.2$ and performed the same procedure as described above. We found for the two populations a slightly different relative age ($\Delta_{AGE} = 70 \pm 110$ Myr). We thus confirm that the two populations have a difference in age

Table 3. Summary of all the uncertainties on Δ_{AGE}

Parameter	Variation	$\sigma_{\Delta AGE}$
Photometry		±110 Myr
ΔY	±0.006	∓40 Myr
[Fe/H]	±0.02	±200 Myr
[α/Fe]	±0.02	±150 Myr
C+N+O	∂AGE/∂[CNO] ~ -3.3 Gyr dex^{-1}	

within ∼110 Myr and that the adopted values of [Fe/H] and [α/Fe] do not change our conclusions.

In addition to the photometric error, we also considered the uncertainty in ΔY, that in the previous section we estimated to be 0.006 dex (see Table 2). In order to estimate how this error affects the measure of Δ_{AGE}, we iterated the same procedure previously described, using for POPa the same set of isochrones, and for POPb two additional sets of isochrones with the same [Fe/H] = −0.67 and [α/Fe] = +0.4 as for POPa, but with two different helium enhancements: $\Delta Y = 0.029 + 0.006 = 0.035$ and $\Delta Y = 0.029 - 0.006 = 0.023$. We found that an error of 0.006 dex in ΔY translates into an uncertainty in Δ_{AGE} of $\sigma_{\Delta AGE}(Y) = 40$ Myr.

The AGB and FRMS models predict that the stars of SG have the same [Fe/H] and [α/Fe] of stars of FG, as observed in many GCs. Moreover, the spectroscopic results by Feltzing et al. (2009) confirm that in NGC 6352 the stars of the two populations should have the same metallicity (within 0.02 dex). In any case, we also considered the cases in which POPb has different [Fe/H] or [α/Fe] with respect to POPa, to study the impact of these variations on Δ_{AGE}. As first test, we considered the case in which POPb has metallicity $[Fe/H]_{POPb} = [Fe/H]_{POPa} \pm 0.02$ dex, consistent with the results by Feltzing et al. (2009). We performed the procedure described above using for POPa a set of isochrones with [Fe/H] = −0.67, [α/Fe] = 0.4 and primordial helium, and for POPb [Fe/H] = −0.65, [α/Fe] = 0.4, and $Y = 0.285$. We found that the relative age between the two populations is $\Delta_{AGE} = 210$ Myr. In the same way, we considered for POPb a set of isochrones with the same parameters, except the metallicity that we set at [Fe/H] = −0.69. In this case, we found $\Delta_{AGE} = -190$ Myr. Therefore, a variation on the metallicity of the second population of δ[Fe/H]=±0.02 dex translates in a variation on Δ_{AGE} of $\sigma_{\Delta AGE}([Fe/H]) = \pm 200$ Myr.

We then considered the impact of the α-enhancement variations on the estimate of Δ_{AGE}. Similarly to what was done already for the variations in metallicity, we considered a set of isochrones for POPa with [Fe/H] = −0.67, [α/Fe] = 0.4 and $Y = 0.256$, and for POPb the same [Fe/H], enhanced in helium by $\Delta Y = 0.029$ and δ[α/Fe] = ±0.02 with respect to POPa. We found that a variation of δ[α/Fe]=±0.02 dex leads to a variation on Δ_{AGE} of $\sigma_{\Delta AGE}([\alpha/Fe]) = \pm 150$ Myr.

It is possible that POPa and POPb have different C+N+O abundances. Unfortunately, we are not able to directly verify the effects of C+N+O abundances variations on the estimate of Δ_{AGE}. Marino et al. (2012b) presented a [Fe/H]-independent relation between the C+N+O variations and the age of a population ∂AGE/∂[CNO] ~ -3.3 Gyr dex^{-1}. If the POPb is CNO-enhanced with respect the POPa, then POPb is younger compared to the case in which both populations have the same CNO abundances, and therefore Δ_{AGE} is larger. However, we note that the m_{F814W} and $(m_{F606W} - m_{F814W})$ magnitude and colour on which our analysis is based are the least affected by C, N, O variations.

In Table 3, we provide a summary of all the uncertainties on Δ_{AGE} introduced by the variation of the considered parameters.

7 CONCLUSIONS

In this paper, we have presented an analysis of the CMDs and two-colour diagrams from WFC3/UVIS *F*275*W*, *F*336*W* and *F*438*W*, and ACS/WFC *F*625*W*, *F*658*N*, *F*606*W* and *F*814*W* photometry.

We identified two stellar populations (named POPa and POPb), that, with appropriate combinations of magnitudes and colours, we could clearly distinguish on most of the evolutionary sequences of the CMD, from the MS, to the SGB, RGB, AGB, and HB.

Using a multicolour analysis method, we have already applied to half a dozen of other GCs, we estimated a $\Delta Y = 0.029 \pm 0.006$ between the two populations.

We also developed a new procedure (similar to that developed by Joo & Lee 2013) for evaluating the difference in age between the two populations hosted by NGC 6352. We considered the filter combinations that are the least affected by light-element variations. We studied the case in which POPa and POPb have the same [Fe/H], as inferred from high-resolution spectroscopy by Feltzing et al. (2009), but POPb has helium abundance enhanced by $\Delta Y = 0.029 \pm 0.006$. We found that the two populations have a difference in age between the POPa and POPb of $\Delta_{AGE} = 10 \pm 110$ Myr, where the error includes the photometric error and the error on the fit. The error in ΔY leads to an error on the relative age of $\sigma_{\Delta AGE} = \pm 40$ Myr, and a total error of 120 Myr. This is the best relative ages between the two populations we can estimate assuming that the two populations have the same [Fe/H] and [α/Fe].

In the case that POPb has a different [Fe/H] content of ± 0.02 dex (as suggested by high-resolution spectroscopy by Feltzing et al. 2009), the relative ages would change by ±200 Myr. For a difference in [α/Fe] of ±0.02 dex, we found a Δ_{AGE} variation of ±150 Myr. As shown by Marino et al. (2012b), if POPb is CNO-enhanced then it must be younger since the turn-off brightness is the same. Differences in metallicity between two populations hosted by a normal GC, however, are not predicted by 'AGB' and 'FRMS' models of formation of multiple stellar populations and are also not observed for this cluster.

In literature, there are numerous works on the relative age of multiple stellar populations hosted by anomalous GCs for which a spread in metallicity is measured. Surely, the most controversial case is represented by ω Centauri. Sollima et al. (2008) identified four coeval populations with different metallicities and helium contents, while Villanova et al. (2014) identified a large spread in age for each population and found that the most metal-rich population also is the oldest one, concluding that ω Centauri is the result of a merger of two different progenitors. Marino et al. (2012a) found that the populations of M 22, characterized by different metallicities, are almost coeval within ∼300 Myr. Lee et al. (2013) found that the GC NGC 2419 hosts two populations characterized by a large difference in [Fe/H], *Y* and with a relative age of about 2 Gyr. Roh et al. (2011) compared models and CMDs of NGC 288 to put constraints on the second stellar population hosted by this GC. They found that, in order to properly reproduce the observed CMDs, the SG must be moderately metal enhanced by 0.16 dex, helium-enhanced by 0.03 dex, and younger by 1.5 Gyr than the FG.

The work we present in this paper is different from previous studies on the relative ages of multiple stellar populations in GCs, in the sense that this is the first attempt to measure relative ages within a multiple population GC with no observed signature of [M/H] dispersion. Assuming no difference in [Fe/H], [α/Fe], and C+N+O content, the two populations of NGC6352 have a 1σ spread in age ∼120 Myr. A combination of small differences in [Fe/H] and [α/Fe] of 0.02 dex would rise the total uncertainty on the relative age to ∼280 Myr (within which the two populations are still coeval).

ACKNOWLEDGEMENTS

DN is supported by a grant 'Borsa di studio per l'estero, bando 2013' awarded by 'Fondazione Ing. Aldo Gini' in Padova (Italy). SC, SO, and GP acknowledge partial support by PRIN-INAF 2014. SO and GP acknowledge partial support by Progetto di Ateneo (Università di Padova) 2014. APM acknowledges support by the Australian Research Council through Discovery Early Career Researcher Award DE150101816.

REFERENCES

Anderson J. et al., 2008, AJ, 135, 2114
Bastian N., Lamers H. J. G. L. M., de Mink S. E., Longmore S. N., Goodwin S. P., Gieles M., 2013, MNRAS, 436, 2398
Behr B. B., 2003, ApJS, 149, 67
Bellini A., Bedin L. R., Piotto G., Milone A. P., Marino A. F., Villanova S., 2010, AJ, 140, 631
Carretta E., Gratton R. G., 1997, A&AS, 121, 95
Carretta E., Bragaglia A., Gratton R., D'Orazi V., Lucatello S., 2009, A&A, 508, 695
D'Antona F., Caloi V., Montalbán J., Ventura P., Gratton R., 2002, A&A, 395, 69
D'Antona F., Bellazzini M., Caloi V., Pecci F. F., Galleti S., Rood R. T., 2005, ApJ, 631, 868
D'Antona F., Ventura P., Decressin T., Vesperini E., D'Ercole A., 2014, MNRAS, 443, 3302
D'Ercole A., D'Antona F., Ventura P., Vesperini E., McMillan S. L. W., 2010, MNRAS, 407, 854
D'Ercole A., D'Antona F., Carini R., Vesperini E., Ventura P., 2012, MNRAS, 423, 1521
Decressin T., Meynet G., Charbonnel C., Prantzos N., Ekström S., 2007, A&A, 464, 1029
di Criscienzo M., D'Antona F., Ventura P., 2010, A&A, 511, A70
Dotter A., Chaboyer B., Jevremović D., Kostov V., Baron E., Ferguson J. W., 2008, ApJS, 178, 89
Dupree A. K., Avrett E. H., 2013, ApJ, 773, L28
Dupree A. K., Strader J., Smith G. H., 2011, ApJ, 728, 155
Feltzing S., Primas F., Johnson R. A., 2009, A&A, 493, 913
Gratton R., Sneden C., Carretta E., 2004, ARA&A, 42, 385
Harris W. E., 1996, AJ, 112, 1487
Joo S.-J., Lee Y.-W., 2013, ApJ, 762, 36
King I. R. et al., 2012, AJ, 144, 5
Kraft R. P., Sneden C., Langer G. E., Shetrone M. D., 1993, AJ, 106, 1490
Kurucz R. L., 1993, SYNTHE Spectrum Synthesis Programs and Line Data, Kurucz CD-ROM. Smithsonian Astrophysical Observatory, Cambridge, MA
Kurucz R. L., Avrett E. H., 1981, SAO Special Report, 391
Lee Y.-W. et al., 2013, ApJ, 778, L13
Marino A. F., Villanova S., Piotto G., Milone A. P., Momany Y., Bedin L. R., Medling A. M., 2008, A&A, 490, 625
Marino A. F. et al., 2011, A&A, 532, A8
Marino A. F. et al., 2012a, A&A, 541, A15
Marino A. F. et al., 2012b, ApJ, 746, 14
Marino A. F. et al., 2014, MNRAS, 437, 1609
Marks M., Kroupa P., 2010, MNRAS, 406, 2000
Milone A. P., Bedin L. R., Piotto G., Anderson J., 2009, A&A, 497, 755
Milone A. P., Piotto G., Bedin L. R., Cassisi S., Anderson J., Marino A. F., Pietrinferni A., Aparicio A., 2012a, A&A, 537, A77
Milone A. P. et al., 2012b, ApJ, 744, 58
Milone A. P., Marino A. F., Piotto G., Bedin L. R., Anderson J., Aparicio A., Cassisi S., Rich R. M., 2012c, ApJ, 745, 27
Milone A. P. et al., 2013, ApJ, 767, 120
Milone A. P. et al., 2015, MNRAS, 447, 927 (Paper II)
Mucciarelli A., Lovisi L., Lanzoni B., Ferraro F. R., 2014, ApJ, 786, 14
Nardiello D., Milone A. P., Piotto G., Marino A. F., Bellini A., Cassisi S., 2015, A&A, 573, A70
Norris J. E., Da Costa G. S., 1995, ApJ, 441, L81
Pasquini L., Mauas P., Käufl H. U., Cacciari C., 2011, A&A, 531, A35
Pietrinferni A., Cassisi S., Salaris M., Castelli F., 2004, ApJ, 612, 168
Pietrinferni A., Cassisi S., Salaris M., Percival S., Ferguson J. W., 2009, ApJ, 697, 275
Piotto G. et al., 2007, ApJ, 661, L53
Piotto G. et al., 2012, ApJ, 760, 39
Piotto G. et al., 2015, AJ, 149, 91 (Paper I)
Roh D.-G., Lee Y.-W., Joo S.-J., Han S.-I., Sohn Y.-J., Lee J.-W., 2011, ApJ, 733, L45
Salaris M., Cassisi S., 2014, A&A, 566, A109
Sarajedini A. et al., 2007, AJ, 133, 1658
Sbordone L., Bonifacio P., Castelli F., Kurucz R. L., 2004, Mem. Soc. Astron. Ital. Suppl., 5, 93
Sbordone L., Salaris M., Weiss A., Cassisi S., 2011, A&A, 534, A9
Silverman B. W., 1986, Monographs on Statistics and Applied Probability. Chapman and Hall, London
Sollima A., Ferraro F. R., Pancino E., Bellazzini M., 2008, Mem. Soc. Astron. Italiana, 79, 342
Villanova S., Piotto G., Gratton R. G., 2009, A&A, 499, 755
Villanova S., Geisler D., Piotto G., Gratton R. G., 2012, ApJ, 748, 62
Villanova S., Geisler D., Gratton R. G., Cassisi S., 2014, ApJ, 791, 107
Yong D., Grundahl F., 2008, ApJ, 672, L29
Yong D. et al., 2014, MNRAS, 441, 3396

This paper has been typeset from a TEX/LATEX file prepared by the author.